Zero-field dynamics stabilized by in-plane shape anisotropy in MgO-based spin-torque oscillators

Kowalska, E.; Kákay, A.; Fowley, C.; Sluka, V.; Lindner, J.; Fassbender, J.; Deac, A. M.;

Originally published:

February 2019

Journal of Applied Physics 125(2019)8, 083902

DOI: https://doi.org/10.1063/1.5081036

Zero-field dynamics stabilized by in-plane shape anisotropy in MgO-based spin-torque oscillators

E. Kowalska,[1, a)] A. Kákay,[1] C. Fowley,[1] V. Sluka,[1] J. Lindner,[1] J. Fassbender,[1, 2] and A. M. Deac[1]

[1)] *Helmholtz-Zentrum Dresden - Rossendorf, Institute of Ion Beam Physics and Materials Research, Bautzner Landstrasse 400, 01328 Dresden, Germany*

[2)] *Institute of Solid State Physics, TU Dresden, Zellescher Weg 16, 01069 Dresden, Germany*

(Dated: 1 February 2019)

Here we demonstrate numerically that shape anisotropy in MgO-based spin-torque nano-oscillators consisting of an out-of-plane magnetized free layer and an in-plane polarizer is necessary to stabilize out-of-plane magnetization precession without the need of external magnetic fields. As the in-plane anisotropy is increased, a gradual tilting of the magnetization towards the in-plane easy direction is introduced, favouring zero-field dynamics over static in-plane states. Above a critical value, zero-field dynamics are no longer observed. The optimum ratio of in-plane shape to out-of-plane uniaxial anisotropy, for which large angle out-of-plane zero-field dynamics occur within the widest current range, is reported.

I. INTRODUCTION

The discovery of giant magnetoresistance effect by Fert[1] and Grünberg[2] in the late 1980's led to a paradigm shift in the miniaturization of magnetic storage devices which is still visible to the present day. It was not until several years later, that the reciprocal effect, the spin-transfer torque (STT), was theoretically predicted[3,4], and several additional years of technological developments in order for this effect to be experimentally observed[5–7]. This initial demonstration spearheaded a rapidly growing field which includes spin-transfer-torque random access memory (STT-MRAM)[6], and spin-torque nano-oscillators (STNOs). STNOs are potential low input power radio-frequency devices for wireless communication, whose frequency can be adjusted simply by changing the applied electrical bias[7].

While initial studies on spin-transfer driven dynamics were carried out on fully metallic systems with both the free and the reference layers magnetized in-plane[7], hybrid device geometries combining an in-plane (IP) and an out-of-plane (OOP) magnetized layers are presently used[8–11]. This geometry helps to reduce the critical current[12], maximises the output power due to large angle precession[9,10], and can provide functionality regardless of applied magnetic or current history[8,10]. Moreover, since the IP reference layer also acts as a read-out layer, the overall number of layers is reduced, thus simplifying the fabrication process in comparison with the hybrid geometry including an OOP polarizer and an IP free layer and requires a third, reference IP layer for the read-out[13,14]. Such a geometry was also analyzed in detail in Ref.[15] and Ref.[16], where the authors theoretically predict a possibility of several types of zero-field magnetization precessions.

Currently, the STNOs based on magnetic tunnel junctions (MTJs) attract the most interest due to their much higher output powers[10] and lower operation currents[9,17,18] compared to their fully metallic counterparts[7,8]. In terms of prospective applications, it is also desirable that STNOs function without a need for external fields. According to some theoretical models[11,19], for hybrid geometry MTJs, as considered here, there is no current-driven dynamics at zero applied field. It has been recently suggested that the perpendicular (field-like) spin-transfer torque can stabilize dynamics at zero-field[20,21]. Likewise, it was shown that a small in-plane field, which, if intrinsically available due to stray fields, can also stabilize dynamics without externally applied magnetic fields.[22] To the authors' knowledge, however, the zero-field oscillations have been observed for nano-pillars with elliptical cross-sections only.[7,9,18] What is lacking is a comprehensive study regarding the influence of shape anisotropy in the considered system.

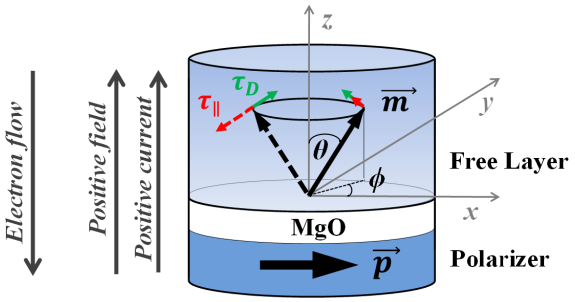

FIG. 1. Considered STNO geometry with marked directions of the positive field and current. The steady-state precession occurs only for electrons flowing from the polarizer to the free layer[9–11,18,19] (positive current flow), which corresponds to the presented configuration of the in-plane spin-transfer torque and the damping torque (marked as $\tau_\parallel$ and τ_D, respectively).

In this paper we analytically and numerically investigate the influence of an in-plane anisotropy component on zero-field out-of-plane dynamics in MgO-based spin-torque nano-oscillators with an OOP magnetized free layer and an IP polarizer (see Fig. 1). We vary the magnitude of the in-plane anisotropy of the system by changing the ellipticity of the free layer cross-section, and investigate its influence on the presence of the OOP steady-state precession over given ranges of applied currents and OOP magnetic fields.

We have previously reported zero-field oscillations stabilized by shape anisotropy in metallic systems. Although

[a)] Electronic mail: e.kowalska@hzdr.de

the effect is similar, here we discuss MTJs, where the spin-transfer-torque asymmetry is entirely the consequence of the angular dependence of the TMR, and the dynamics is also considerably affected by the bias voltage dependence of the spin-transfer torques. The physics allowing for steady-state precession in MTJs is discussed in detail Ref.[19], where we present experimental results and a theoretical model explaining the quenching of dynamics at high bias; nevertheless, the analytical calculations reported in Ref.[19] ignore any in-plane contributions to the effective field. In contrast, here we focus on quantifying the role of the shape anisotropy and the range where it can help sustaining zero-field magnetization dynamics. The work in Ref.[18], focusing on GMR devices, shows qualitatively different trends reflecting the different physical origins of steady-state precession in the two types of STNOs.

We analytically solve the Landau-Lifshitz-Gilbert-Slonczewski (LLGS) equation for a typical device with circular cross-section under perpendicular applied fields and currents. We define the angular asymmetry of the in-plane term of the spin-transfer torque as resulting from the cosine-type dependence of the tunnel magnetoresistance (TMR) on the angle between the magnetizations of the free and the reference layers[25,26] (i.e., **m** and **p** vectors, respectively; see Fig. 1). We take into account the spin-torque bias dependence, as well as the bias dependence of the tunnel magnetoresistance, which, in fact, yields a suppression of the output power at large applied currents (as demonstrated in Ref.[19]). We assume a linear bias dependence of the TMR for the antiparallel (AP) state (R_{AP}) and a constant resistance for the parallel (P) state (R_P)[24,26–29].

II. RESULTS AND DISCUSSION

The motion of the free layer magnetization **m** is described by the LLGS equation[3,17]:

$$\frac{d\mathbf{m}}{dt} = -\gamma(\mathbf{m}\times\mu_0\mathbf{H_{eff}}) + \alpha(\mathbf{m}\times\frac{d\mathbf{m}}{dt}) + \gamma\frac{\partial\tau_{\parallel}}{\partial V}V[\mathbf{m}\times(\mathbf{m}\times\mathbf{n_x})]. \quad (1)$$

Here, γ is the gyromagnetic ratio, $\partial\tau_{\parallel}/\partial V[T/V]$ is the torkance of the in-plane STT term[30,31], α is a Gilbert damping constant, $\mathbf{n_x}$ and $\mathbf{n_z}$ are the unit vectors of the coordinate system presented in Fig. 1. The effective magnetic field is defined as $\mu_0\mathbf{H_{eff}} = \mu_0 H_{ext}\mathbf{n_z} + \mu_0 H_{k_\perp} m_z \mathbf{n_z} + \mu_0 H_{k_\parallel} m_x \mathbf{n_x}$, where $\mu_0 H_{ext}$ is the external field, $\mu_0 H_{k_\perp}$ is the effective out-of-plane anisotropy along the z-axis ($\mu_0 H_{k_\perp} = \mu_0 H_k - \mu_0 M_S$, where $\mu_0 H_k$ is an uniaxial magnetic anisotropy field and M_s is a saturation magnetization), and $\mu_0 H_{k_\parallel}$ is the effective in-plane shape anisotropy along the x-axis.

We define a linear bias dependence of the resistance difference ΔR between the P and the AP states as follows: $\Delta R = -(\partial R_{AP}/\partial V)\times|V| + \Delta R_0$ (here, ΔR_0 is the resistance difference between the two states close to zero bias, and $\partial R_{\rm AP}\partial V$ is the slope of the linear bias dependence of the AP state resistance)[24]. For each instant angle between the magnetic moments of two layers, we convert the current i into an equivalent voltage value V, as we have previously proposed in Ref.[19]. In order to estimate the onset current for precession, we consider the limit of small precession angles θ (i.e., $\theta \to 0$ for positive applied fields and $\theta \to \pi$ for negative applied fields), and we solve the LLGS equation (1) expressed in the spherical coordinates, as discussed in detail in Ref.[19]. We obtained the following analytical equation defining the region of the out-of-plane steady-state precession:

$$\mu_0 H_{ext(\theta\to 0)}(i) < \left| \frac{\frac{\partial\tau_{\parallel}}{\partial V}\left(\Delta R_0 - |i|\frac{\partial R_{AP}}{\partial V}R_P\right)}{\alpha\left(2+|i|\frac{\partial R_{AP}}{\partial V}\right)^2} i - \mu_0 H_{k_\perp} + \mu_0 H_{k_\parallel} \right|. \quad (2)$$

For $\mu_0 H_{k_\parallel} = 0$, at low applied fields, the in-plane STT stabilizes the static in-plane antiparallel state within a region of the phase diagram defined as follows[24]:

$$\mu_0 H_{ext}(i) \le \left| \frac{\partial\tau_{\parallel}}{\partial V} R_P i \right|. \quad (3)$$

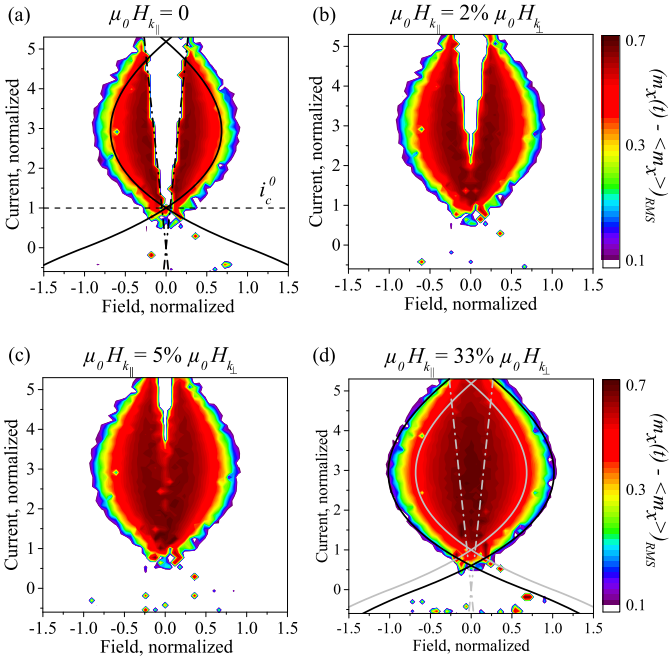

FIG. 2. Current versus field dynamic state diagrams: (a) for a nanopillar with circular cross-section ($\mu_0 H_{k_\parallel} = 0$), and for one with elliptical cross-section where (b) $\mu_0 H_{k_\parallel} = 2\%\,\mu_0 H_{k_\perp}$, (c) $\mu_0 H_{k_\parallel} = 5\%\,\mu_0 H_{k_\perp}$, (d) $\mu_0 H_{k_\parallel} = 33\%\,\mu_0 H_{k_\perp}$. Coloured area shows numerically determined intensity of magnetization dynamics along x-axis. Black solid lines in (a) and (d) show analytical solution determining the region of steady state precession (eq. 2). Dashed lines in (a) determine the stability region of static IP state for the case of $\mu_0 H_{k_\parallel} = 0$ (eq. 3). For the comparison, grey solid and dashed lines in (d) show the analytical solution for the case shown in (a).

In order to prove the validity of the analytical solutions, the numerical integration of eq. 1 was also performed. We used the MAPLE 8 program and the

simulation parameters typical for the considered system: $\partial\tau_{\parallel}/\partial V = 0.00672\,T/V$[32], $\alpha = 0.005$[33], $\Delta R_0 = 100\,\Omega$[24], $R_P = 200\,\Omega$[24], $\mu_0 H_{k_\perp} = 200\,mT$, and $\partial R_{AP}\partial V = 10\,\Omega/V$. The simulation time was set to 150 ns and the initial magnetization position was random. The final static and dynamic states were defined based on the last 2 ns of the simulation.

Fig. 2 shows numerically determined field versus current dynamic phase diagrams calculated for free layers with different cross-sectional ellipticities. The coloured areas show the intensity of magnetization dynamics along the x-axis, expressed as the root mean square (RMS) of $(m_x(t) - \langle m_x \rangle)$ (where $m_x(t)$ and $\langle m_x \rangle$ are the instantaneous and the mean m_x value, respectively). In a real device, these values directly correlate with the generated output power of the spin-torque nano-oscillator.[23] Normalized current values are defined as i/i_c^0, where i_c^0 is the current value at the crossing of the analytically determined critical lines for dynamics for the case of a nano-pillar with circular cross-section (as marked with dashed line in Fig. 2(a)). Field values are normalized by the effective out-of-plane anisotropy, $\mu_0 H_{k_\perp}$.

The dynamic diagram for the case of the circular cross-section, i.e. when the in-plane anisotropy component is equal to zero ($\mu_0 H_{k_\parallel} = 0$), is presented in Fig. 2(a). Our results show that stable dynamics occur only for positive currents, defined as electrons flowing from the free to the reference layer[9–11,18,19]. This is a consequence of the fact that, in most MTJs, $\mathrm{STT}_\parallel$ is larger close to the AP state and, thus, more capable of overcoming the damping torque[24] (see a sketch of precession mechanism in Fig. 1). As shown in Fig. 2(a), with increasing applied field, the onset current for dynamics initially increases quasi-parabolically. Above a certain current value (here, for $i = 3i_c^0$), we observe a quenching of STNO dynamics and a reduction of the dynamic region, which is a direct effect of the TMR bias dependence[24]. We also observe a gap in the dynamics at zero and low applied field, where the antiparallel static state is stabilized[24]. The analytical solution defining the area of out-of-plane dynamics (eq. 2) and the static in-plane state (eq. 3) are plotted in Fig. 2(a) with solid and dashed lines respectively, and accurately define the regions of numerically obtained out-of-plane dynamics.

We now define the ellipticity of the free layer by introducing the in-plane shape anisotropy, $\mu_0 H_{k_\parallel}$, expressed in the percentage of the effective out-of-plane anisotropy, $\mu_0 H_{k_\perp}$. While increasing $\mu_0 H_{k_\parallel}$ from 2% (Fig. 2(b)) to 5% (Fig. 2(c)) of $\mu_0 H_{k_\perp}$, the dynamic gap from Fig. 2(a) gradually closes and zero-field dynamics are stabilized over the entire current range for $\mu_0 H_{k_\parallel} = 10\%\ \mu_0 H_{k_\perp}$. This is the effect of the gradual tilting of the magnetization towards the in-plane easy direction (x-axis) which enables the onset angle for precession to be reached at lower electrical currents, leading to stable magnetization dynamics and a suppression of the critical behaviour of the stabilization of static AP state. Further increase of $\mu_0 H_{k_\parallel}$ leads to the largest intensity of zero-field magnetization dynamics at $\mu_0 H_{k_\parallel} = 33\%\ \mu_0 H_{k_\perp}$ (see Fig. 2(d)). We also observe here a pronounced expansion of the dynamic region along the field axis, which can be easily distinguished by comparing the plotted analytical lines of these two cases (i.e., the black and the grey lines in Fig. 2(d), showing the analytical solutions for $\mu_0 H_{k_\parallel} = 33\%\ \mu_0 H_{k_\perp}$ and $\mu_0 H_{k_\parallel} = 0$, respectively).

The comparison between the shapes of the magnetization precession trajectories for different $\mu_0 H_{k_\parallel}$ values is presented in Fig. 3(a) and (b). Fig. 3(a) shows concentric projections of the precession trajectories on the xy-plane, where the ellipticity increases with the increasing $\mu_0 H_{k_\parallel}$. We can see a gradual decrease of the maximum m_x and m_y components, with a more pronounced reduction of m_y. 3-dimensional plots in Fig. 3(b) shows the real shapes of the trajectories, which are transforming from circular (black trajectory) to out-of-plane clam-shell-type (blue trajectory) while increasing $\mu_0 H_{k_\parallel}$ from $\mu_0 H_{k_\parallel} = 2\%\ \mu_0 H_{k_\perp}$ to $\mu_0 H_{k_\parallel} = 84\%\ \mu_0 H_{k_\perp}$. This directly shows how the anisotropy energy, arising from the introduced elliptical shape of the nano-pillar, acts on the magnetization by pushing it away from the in-plane magnetic hard axis, oriented along the y-axis, similar to what is obtained in equivalent metallic systems[23].

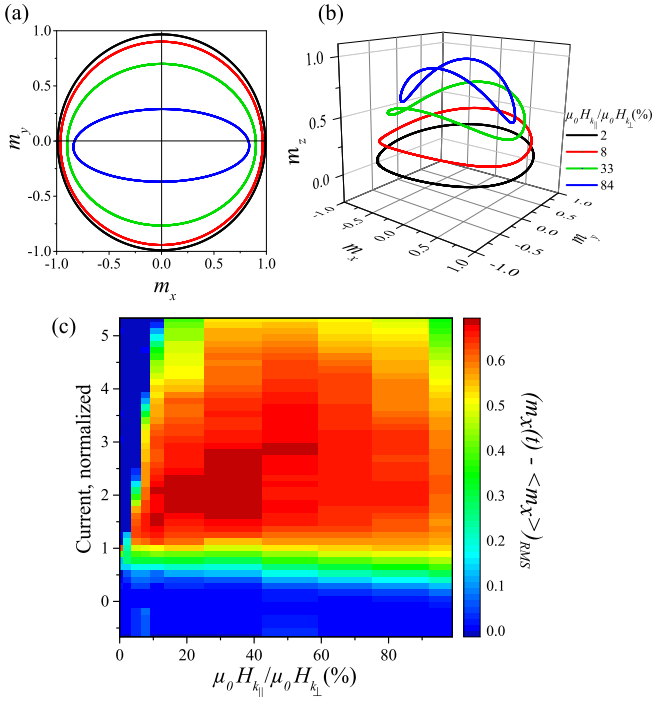

FIG. 3. Zero-field magnetization dynamics for $0 < \mu_0 H_{k_\parallel} < \mu_0 H_{k_\perp}$. Magnetization precession trajectories at $i = 1.9 i_c^0$ for different $\mu_0 H_{k_\parallel}$ values: (a) projections of trajectories on xy-plane, (b) trajectories in xyz space. (c), Intensity of magnetization dynamics as a function of the applied current and $\mu_0 H_{k_\parallel}/\mu_0 H_{k_\perp}$ expressed in percentage.

Fig. 3(c) shows the intensity of zero-field magnetization dynamics along the x-axis as a function of $\mu_0 H_{k_\parallel}/\mu_0 H_{k_\perp}$ (in %) and the current. The minimum current required to observe dynamics is reduced gradually by around $i/i_c^0 = 0.3$ as $\mu_0 H_{k_\parallel}$ is increased from $\mu_0 H_{k_\parallel} = 0$ to $\mu_0 H_{k_\parallel} = 100\%\ \mu_0 H_{k_\perp}$. Maximum operation currents (i.e., high currents still driving dynamics) initially increase with increasing $\mu_0 H_{k_\parallel}$, up to

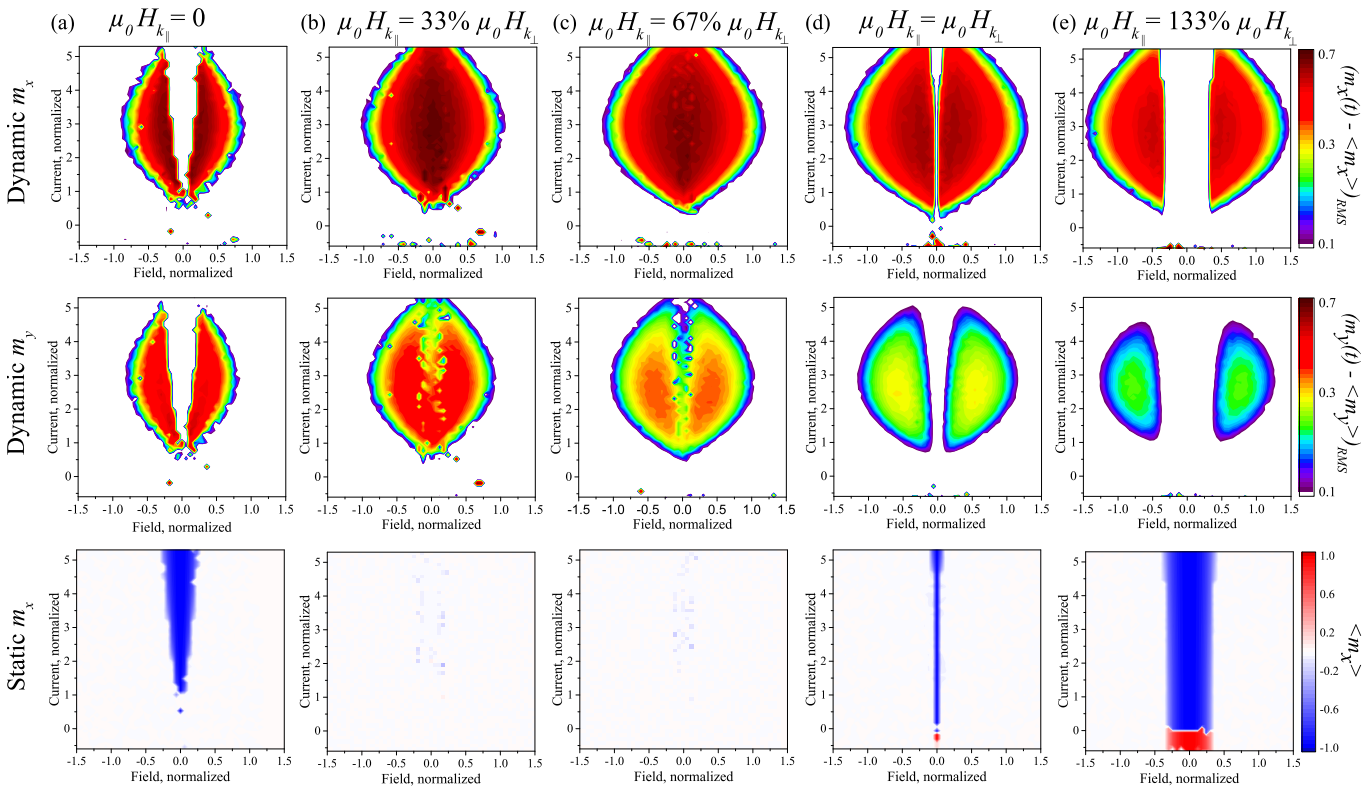

FIG. 4. Dynamic and static phase diagrams for: (a) $\mu_0 H_{k_\parallel} = 0$, (b) $\mu_0 H_{k_\parallel} = 33\%\ \mu_0 H_{k_\perp}$, (c) $\mu_0 H_{k_\parallel} = 67\%\ \mu_0 H_{k_\perp}$, (d) $\mu_0 H_{k_\parallel} = \mu_0 H_{k_\perp}$, and (e) $\mu_0 H_{k_\parallel} = 133\%\ \mu_0 H_{k_\perp}$. First row: corresponding phase diagrams showing the intensity of magnetization dynamics along the x-axis, translating directly into the output power of the STNO device. Second row: corresponding phase diagrams of the intensity of magnetization dynamics along the y-axis, reflecting a progressing deformation of the magnetization precession trajectory with increasing $\mu_0 H_{k_\parallel}$. Third row: corresponding phase diagrams of the static in-plane state, showing an average magnetization along the x-axis; here, the region of $\langle m_x \rangle = -1$ represents the static in-plane AP state.

the $\mu_0 H_{k_\parallel} = 50\%\ \mu_0 H_{k_\perp}$, and then decreases. We also observe a general increase of the intensity of magnetization dynamics up to $\mu_0 H_{k_\parallel} = 35\%\ \mu_0 H_{k_\perp}$, followed by a decrease as $\mu_0 H_{k_\parallel}$ further increases. According to Fig. 3(c), the in-plane anisotropy should be then optimized for both low onset currents and large operation current ranges, simultaneously still maintaining high output power zero-field dynamics of the device. We found the optimum value of $\mu_0 H_{k_\parallel} = 33\%\ \mu_0 H_{k_\perp}$, where the large intensity of zero-field magnetization dynamics were observed within the widest current range and the maximum $(m_x(t) - \langle m_x \rangle)_{RMS} \approx 0.7$ was obtained for the largest current range of $1.5 < i/i_c^0 < 3$). Note that the dynamic diagram for $\mu_0 H_{k_\parallel} = 33\%\ \mu_0 H_{k_\perp}$ is also presented in Fig. 2(d).

Fig. 4 shows the effect of the increasing in-plane shape anisotropy, $\mu_0 H_{k_\parallel}$, on the out-of-plane dynamics along the x-axis, $(m_x(t) - \langle m_x \rangle)_{RMS}$ (the first row), and along the y-axis, $(m_y(t) - \langle m_y \rangle)_{RMS}$ (the second row), as well as on the stability region of static in-plane states, represented by an average m_x component, $\langle m_x \rangle$ (the third row). With increasing $\mu_0 H_{k_\parallel}$, we observe a general reduction of intensity of magnetization dynamics along the x-axis (see the first row), translating into the loss of the output power in the actual STNO device. This is consistent with the evolution of the shape of the magnetization trajectory presented above, which shows that the maximum value of m_x decreases (see trajectory projections in Fig. 3(a)) once the trajectory changes its shape from circular to clam-shell-type (as shown in Fig. 3(b)). This also explains the significant reduction of the intensity of magnetization dynamics along the y-axis (see the second row in Fig. 4), occurring due to the described deformation of the precession trajectory.

The third row in Fig. 4 shows the corresponding average magnetization along the x-axis. Here, the blue areas represent the stability regions of the static AP state (for $\langle m_x \rangle = -1$). For a free layer with circular cross-section, shown in Fig. 4(a), at small applied fields, positive currents stabilize the static in-plane AP state. For the cases of $\mu_0 H_{k_\parallel} = 33\%\ \mu_0 H_{k_\perp}$ and $\mu_0 H_{k_\parallel} = 67\%\ \mu_0 H_{k_\perp}$ (the third row of Fig. 4 (b) and (c)), the in-plane anisotropy stabilizes zero-field dynamics, replacing the area of the static AP state. When $\mu_0 H_{k_\parallel} = \mu_0 H_{k_\perp}$ (Fig. 4(d)) or $\mu_0 H_{k_\parallel} > \mu_0 H_{k_\perp}$ (Fig. 4(e)), no dynamics are obtained at zero-field (neither along x- nor y-axis), and the static AP state at $\langle m_x \rangle = -1$ is instead stabilized. We additionally observe the presence of an onset field for out-of-plane dynamics which is, in fact, slightly larger than the difference between the two anisotropies, i.e. $\mu_0 H_{onset} \approx \mu_0 H_{k_\parallel} - \mu_0 H_{k_\perp}$. As a result, in the case when $\mu_0 H_{k_\parallel} > \mu_0 H_{k_\perp}$, one should apply an

external out-of-plane field in order to overcome the in-plane anisotropy and pull the magnetization back towards the OOP direction.

III. CONCLUSIONS

To summarize, we numerically and analytically investigate the influence of the in-plane shape anisotropy on zero-field out-of-plane dynamics in MgO-based STNOs with an OOP magnetized free layer and an IP polarizer. As previously reported, we observe no zero-field dynamics for circular nano-pillars of this particular geometry. According to our results, introducing a $\mu_0 H_{k_\parallel}$ constant as low as 2% of $\mu_0 H_{k_\perp}$ is already sufficient for inducing zero-field oscillations, which persist as long as $\mu_0 H_{k_\parallel} < \mu_0 H_{k_\perp}$. Initially, the oscillations are restricted to a narrow current range, which increases as $\mu_0 H_{k_\parallel}$ increases, covering the whole dynamic range for $\mu_0 H_{k_\parallel} = 10\%\, \mu_0 H_{k_\perp}$. We found the optimum value of $\mu_0 H_{k_\parallel} = 33\%\, \mu_0 H_{k_\perp}$, for which large angle out-of-plane zero-field dynamics occur within the widest current range (e.g., $\mu_0 H_{k_\perp} = 100\,\text{mT}$ and $\mu_0 H_{k_\parallel} = 33\,\text{mT}$ would correspond to the free layer dimensions of $260 \times 72 \times 1.3\,\text{nm}$, where 260 nm and 72 nm are long and short axes of the ellipse, respectively, and 1.3 nm is the layer thickness). When $\mu_0 H_{k_\parallel} \geq \mu_0 H_{k_\perp}$, the anisotropy stabilizes the static in-plane AP state at zero-field, which prevents precession. Dynamics can be recovered by the application of a critical field $\mu_0 H_{onset}$ which is approximately equal to $\mu_0 H_{k_\parallel} - \mu_0 H_{k_\perp}$. We also observed a general decrease of the intensity of magnetization dynamics with increasing ellipticity, which is assigned to a gradual change of the magnetization precession trajectory from the circular to clam-shell-type. Consequently, the shape of STNO nano-pillars should be taken into account while designing an actual commercial device; in particular, in terms of the presence of zero-field dynamics itself, but also in order to maximize the output power, minimize the operation currents, or tune the operation current range.

ACKNOWLEDGMENTS

This research was supported by the Helmholtz Young Investigator Initiative Grant No. VH-N6-1048. The authors would like to thank Dr. Kai Wagner for fruitful discussions.

[1] M. N. Baibich, J. M. Broto, A. Fert, F. Nguyen Van Dau, F. Petroff, P. Etienne, G. Creuzet, A. Friederich, and J. Chazelas, "Giant magnetoresistance of (001)Fe/(001)Cr magnetic superlattices", Phys. Rev. Lett. **61**, 21 (1988).

[2] G. Binasch, P. Grünberg, F. Saurenbach, and W. Zinn, "Enhanced magnetoresistance in layered magnetic structures with antiferromagnetic interlayer exchange", Phys. Rev. B **39**, 7 (1989).

[3] J. C. Slonczewski, "Current-driven excitation of magnetic multilayers", J. Magn. Magn. Mater. **159**, L1-L7 (1996).

[4] L. Berger, "Emission of spin waves by a magnetic multilayer traversed by a current", Phys. Rev. B **54**, 9353-9358 (1996).

[5] M. Tsoi, A. G. M. Jansen, J. Bass, W-C. Chiang, M. Seck, V. Tsoi, and P. Wyder, "Excitation of a magnetic multilayer by an electric current", Phys. Rev. Lett. **80**, 4281 (1998).

[6] J. A. Katine, F. J. Albert, R. A. Buhrman, E. B. Myers, and D. C. Ralph, "Current-driven magnetization reversal and spin-wave excitations in Co/Cu/Co pillars", Phys. Rev. Lett. **84**, 3149 (2000).

[7] S. I. Kiselev, J. C. Sankey, I. N. Krivorotov, N. C. Emley, R. J. Schoelkopf, R. A. Buhrman, and D. C. Ralph, "Microwave oscillations of a nanomagnet driven by a spin-polarized current", Nature **425**, 380 (2003).

[8] W. H. Rippard, A. M. Deac, M. R. Pufall, J. M. Shaw, M. W. Keller, S. E. Russek, G. E. W. Bauer, and C. Serpico, "Spin-transfer dynamics in spin valves with out-of-plane magnetized CoNi free layers", Phys. Rev. B **81**, 014426 (2010).

[9] Z. Zeng, G. Finocchio, B. Zhang, P. K. Amiri, J. A. Katine, I. N. Krivorotov, Y. Huai, J. Langer, B. Azzerboni, K. L. Wang, and H. Jianget, "Ultralow-current-density and bias-field-free spin-transfer nano-oscillator", Sci. Rep. **3**, 1426 (2013).

[10] H. Kubota, K. Yakushiji, A. Fukushima, S. Tamaru, M. Konoto, T. Nozaki, S. Ishibashi, T. Saruya, S. Yuasa, T. Taniguchi, H. Arai, and H. Imamura, "Spin-torque oscillator based on magnetic tunnel junction with a perpendicularly magnetized free layer and in-plane magnetized polarizer", Appl. Phys. Express **6**, 103003 (2013).

[11] T. Taniguchi, H. Arai, S. Tsunegi, S. Tamaru, H. Kubota, and H. Imamura, "Critical field of spin torque oscillator with perpendicularly magnetized free layer", Appl. Phys. Express **6**, 123003 (2013).

[12] S. Mangin, D. Ravelosona, J. A. Katine, M. J. Carey, B. D. Terris, and E. E. Fullerton, "Current-induced magnetization reversal in nanopillars with perpendicular anisotropy", Nat. Mater. **5**, 210-215 (2006).

[13] A. D. Kent, B. Özyilmaz, and E. Del Barco, "Spin-transfer-induced precessional magnetization reversal", Appl. Phys. Lett. **84**, 3897 (2004).

[14] D. Houssameddine, U. Ebels, B. Delaët, B. Rodmacq, I. Firastrau, F. Ponthenier, M. Brunet, C. Thirion, J.-P. Michel, L. Prejbeanu-Buda, M.-C. Cyrille, O. Redon, and B. Dieny, "Spin-torque oscillator using a perpendicular polarizer and a planar free layer", Nature materials **6**, 447 (2007).

[15] D. Pinna, A. D. Kent, and D. L. Stein, "Thermally assisted spin-transfer torque dynamics in energy space", Phys. Rev. B **88**, 104405 (2013).

[16] D. Pinna, D. L. Stein, and A. D. Kent, "Spin-torque oscillators with thermal noise: A constant energy orbit approach", Phys. Rev. B **90**, 174405 (2014).

[17] A. M. Deac, A. Fukushima, H. Kubota, H. Maehara, Y. Suzuki, S. Yuasa, Y. Nagamine, K. Tsunekawa, D. D. Djayaprawira, and N. Watanabe, "Bias-driven high-power microwave emission from MgO-based tunnel magnetoresistance devices", Nat. Phys. **4**, 308 (2008).

[18] W. Skowroński, T. Stobiecki, J. Wrona, G. Reiss, and S. Van Dijken, "Zero-field spin torque oscillator based on magnetic tunnel junctions with a tilted CoFeB free layer", Appl. Phys. Express **5**, 063005 (2012).

[19] T. Taniguchi, H. Arai, H. Kubota, and H. Imamura, "Theoretical study of spin-torque oscillator with perpendicularly magnetized free layer", IEEE Trans. Magn. **50**, 1400404 (2014).

[20] T. Taniguchi, S. Tsunegi, H. Kubota, and H. Imamura, "Self-oscillation in spin torque oscillator stabilized by field-like torque", Appl. Phys. Lett. **104**, 152411 (2014).

[21] Y.-Y. Guo, H.-B. Xue, and Z.-J. Liu, "Oscillation characteristics of zero-field spin transfer oscillators with field-like torque", AIP Adv. **5**, 057114 (2015).

[22] T. Taniguchi, T. Ito, Y. Utsumi, S. Tsunegi, and H. Kubota, "Stable oscillation in spin torque oscillator excited by a small in-plane magnetic field", J. Appl. Phys. 118, 053903 (2015).

[23] C. Fowley, V. Sluka, K. Bernert, J. Lindner, J. Fassbender, W. H. Rippard, M. R. Pufall, S. E. Russek, and A. M. Deac, "Zero-field spin-transfer oscillators combining in-plane and out-of-plane magnetized layers", Appl. Phys. Express **7**, 043001 (2014).

[24] E. Kowalska, A. Fukushima, V. Sluka, C. Fowley, A. Kákay, Y. Aleksandrov, J. Lindner, J. Fassbender, S. Yuasa, and A. M. Deac, "Tunnel magnetoresistance angular and bias dependence enabling tuneable wireless communication", arXiv:1808.10812.

[25] J. C. Slonczewski, "Conductance and exchange coupling of two ferromagnets separated by a tunneling barrier", Phys. Rev. B **39**, 10 (1989).

[26] J. S. Moodera, and L. R. Kinder, "Ferromagnetic–insulator–ferromagnetic tunneling: Spin-dependent tunneling and large magnetoresistance in trilayer junctions", J. Appl. Phys. **79**, 8 (1996).

[27] J. C. Slonczewski, "Currents, torques, and polarization factors in magnetic tunnel junctions", Phys. Rev. B **71**, 024411 (2005).

[28] L. Gao, X. Jiang, S.-H. Yang, J. D. Burton, E. Y. Tsymbal, and S. S. P. Parkin, "Bias voltage dependence of tunneling anisotropic magnetoresistance in magnetic tunnel junctions with mgo and Al_2O_3 tunnel barriers,", Phys. Rev. Lett. **99**, 226602 (2007).

[29] A. Kalitsov, P.-J. Zermatten, F. Bonell, G. Gaudin, S. Andrieu, C. Tiusan, M. Chshiev, and J. P. Velev, "Bias dependence of tunneling magnetoresistance in magnetic tunnel junctions with asymmetric barriers", J. Phys.: Condens. Matter **25**, 496005 (2013).

[30] I. Theodonis, N. Kioussis, A. Kalitsov, M. Chshiev, and W. H. Butler, "Anomalous bias dependence of spin torque in magnetic tunnel junctions", Phys. Rev. Lett. **97**, 237205 (2006).

[31] H. Kubota, A. Fukushima, K. Yakushiji, T. Nagahama, S. Yuasa, K. Ando, H. Maehara, Y. Nagamine, K. Tsunekawa, D. D. Djayaprawira, N. Watanabe, and Y. Suzuki, "Quantitative measurement of voltage dependence of spin-transfer torque in MgO-based magnetic tunnel junctions", Nat. Phys. **4**, 37-41 (2008).

[32] C. Heiliger and M. D. Stiles, "Ab initio studies of the spin-transfer torque in magnetic tunnel junctions", Phys. Rev. Lett. 100, 186805 (2008). **81**, 134419 (2010).

[33] A. Okada, S. Kanai, M. Yamanouchi, S. Ikeda, F. Matsukura, and H. Ohno, "Electric-field effects on magnetic anisotropy and damping constant in Ta/CoFeB/MgO investigated by ferromagnetic resonance", Appl. Phys. Lett. **105**, 052415 (2014).